Faculty of Physics
Babes-Bolyai University

Doctoral Thesis Summary

Designing new plasmonic nanoparticles and photoactive molecules for bioimaging and cancer therapy

by

Sanda Cosmina Boca

Scientific Advisor
Prof. Dr. Simion Astilean

CLUJ-NAPOCA
2011

Contents

Introduction

The major scope of this thesis is to design gold nanoparticles-polymeric conjugates which can serve to intracellular detection and are able to assist with cancer therapy by plasmon heating.

The first chapter presents a short review of the scientific literature regarding the biomedical applications of nanotechnology. The interaction of nanoparticles with living cells is presented, followed by the description of current strategies for cancer diagnosis and treatment in general, with the implication of noble metal nanoparticles in particular.

In the second chapter, we detail the methods employed to fabricate gold nanoparticles of various shapes and the procedures used for nanoparticle biocompatibilization with polymers (chitosan and thiolated methoxy-poly(ethylene) glycol (mPEG-SH)). The optical, morphological and spectroscopic properties of the particles are investigated using a number of techniques: optical spectroscopy, electron microscopy and Surface-enhanced Raman Spectroscopy (SERS).

Chapter three studies the interaction between single and double stranded oligomers and gold nanoparticles by LSPR colorimetric detection. Then, we demonstrate that self-assembled gold particles on solid substrates are versatile tools for surface-enhanced Raman scattering (SERS) detection of p-aminothiophenol molecule under 633 nm laser line excitation.

In the fourth chapter we employ individual colloidal nanoparticles (gold nanorods and flowerlike) as SERS substrates and carriers for various Raman reporter molecules. We demonstrate the production of SERS active tags, showing a high stability and detectability inside a line of epithelial cells from human retina.

In the fifth chapter we evaluate the biological impact of as prepared nanoparticles on healthy and cancer cells in vitro, in function of their surface chemistry.

Chapter six represents the highlight of this thesis: the demonstration that as prepared noble metal nanoparticles can be explored in cancer treatment. We demonstrate that PEGyalted gold nanorods and chitosan- biofunctionalized silver nanotriangles (Chit-AgNTs) serve as efficient agents for the treatment of tumors by plasmon assisted photothermal heating. In parallel we also prove that some new species of Ru(II) complexes are used as photoactive molecules for the glioma treatment by one and two-photon photodymanic therapy. In the last part of this thesis the conclusions and few selected appendices are presented.

Keywords: *noble metal nanoparticles, surface plasmons, cancer therapy*

Chapter 1

1.1 Strategies for cancer diagnosis and treatment

1.1.1. Conventional methods in cancer diagnosis and therapy

Cancer is suspected based on the symptoms a person might present followed by the results of a physical examination and sometimes the results of screening tests. To confirm that cancer is present, more detailed tests (termed diagnostic tests) are required. Conventional cancer diagnosis depends on cellular pathology (cytopathology) such as tissue biopsy, endoscopy, and imaging, all of them investigating the microscopic cellular appearance [1]. The most precise is biopsy which involves the removal of a sample of the tissue on the abnormal area or sometimes of the whole tumor, followed by cytopathological examination of the sample. Other methods used for cancer diagnosis are endoscopy, X-ray, CT (computed tomography), ultrasonography or MRI (magnetic resonance imaging). The traditional cancer treatment relies on various techniques such as surgery, radiation, hormone therapy and more recently chemotherapy, immunotherapy or their combination [2].

1.1.2. Unconvential methods for cancer treatment employed in current thesis

1.1.2.1 Photodynamic therapy

Photodynamic therapy (PDT) is a two-stage procedure that uses an endocytosed photosensitizer which, stimulated by visible light, produces highly reactive singlet oxygen ($^1O_2$) (type II reaction). This cytotoxic agent is the one responsible for inducing membrane alterations leading finally to cytolysis. Two additional mechanisms are believed to mediate tumor cell destruction by photodynamic therapy: destruction of tumor vasculature and the induction of both inflammatory and immune antitumor reactions [3].

1.1.2.2 Plasmon assisted photothermal therapy

Photothermal therapy (PTT) is a new cancer treatment that uses electromagnetic radiation (most often visible light) and injected contrast agents such as weak emitting dyes [4] which convert the photoenergy into thermal energy and thus kill the cancer cells by protein denaturation, cell necrosis or apoptosis. The basic model for its use is derived in part from Photodynamic therapy (PDT) [5]. Unlike PDT, PTT is a more advantageous technique because it doesn’t require oxygen to interact with the targeted cells and also is

able to use longer wavelength light, which is less energetic and therefore less harmful for the healthier cells.

1.1.2.3 Noble metal nanoparticles in cancer imaging and plasmon-assisted photothermal therapy

In photothermal therapy the irradiated tissue temperature can oftenly rise to 46°C, leading to the inactivation of the normal cellular processes (apoptosis), whereas above 46°C, extensive necrosis occurs. Several methods are employed for inducing therapeutical hyperthermia in the presence of proper agents by applying an alternating magnetic or radiofrequency field, or by laser irradiation, usally with near-infrared light [6]. Light-induced heating of nanoparticles in resonance with their plasmon band seems to be the most efficient since, in contrast to nanoparticle heating in a alternating magnetic feld, lower quantities of nanoparticles are requiredin the later case. Moreover, the plasmon band of these nanoparticles can be adjusted from visible to the near-infrared (NIR) range (820 nm) where optical transmission through tissue is optimal, so deep tissue treatment (~1 cm) is feasible. Few recent examples of such therapeutical approach use metal nanoshells, gold nanorods and nanocages or other anysotropic noble metal nanoparticles, usally embedded in a biocompatible polymeric shell.

1.2 Gold nanoparticles and their properties

Gold nanoparticles are generally defined as discrete particles between 1-100 nm in size, usually being suspended in a fluid (colloidal gold). Also known as *nanogold*, colloidal gold suspension has an intense burgundy red colour (for spherical particles less than 100 nm), or a dirty yellowish colour (for much larger particles) [7].

1.2.1 Surface plasmon absorption and scattering of gold nanoparticles

Due to their small size in the nanoscale range, noble metal nanoparticles (NPs) exhibit very interesting physical and chemical properties [8]. The most striking phenomenon encounterd in these nanoparticles are electromagnetic resonances due to the collective oscillation of the conduction band electrons induced by the electromagnetic field (e.g. laser), termed *plasmon resonances*. These plasmon resonances are responsible for strong nanoparticles absorbtion and scattering and the enhancement of the electromagnetic field in their vicinity.

1.2.2. Amplification of the electromagnetic field in the vicinity of gold nanoparticles

Another main consequence of plasmon excitation is the high electromagnetic field created at the surface of the nanoparticle, which is useful in enhancing the sensitivity of Raman spectroscopy in (bio)molecular detection. It was proved that the Raman scattering by the vibrations of the molecules (in general very weak) is enhanced by orders of magnitude in the presence of metals (copper, silver, gold) with nanoscale roughness. This gave birth to a new, powerful analytical tool, Surface-Enhanced Raman Scattering (SERS), for determining chemical fingerprints of molecules adsorbed or near metallic substrates [9]. In addition to SERS, surface-enhanced, or metal-enhanced fluorescence (MEF) has also been reported for molecules near the surfaces of metallic nanostructures [10].

1.2.3 Applications of Plasmonic Gold Nanoparticles in Sensing, Imaging and SERS Detection

The strong SPR absorption bands of metallic nanoparticles render them useful for many other applications. For example, the sensitivity of the SPR bands to their local environment have made metal nanoparticles attractive candidates as colorimetric sensors for analytes such as DNA, metal ions, antibodies, biomolecules or other bioconjugates [11]. Although less widely exploited than the extinction-based colorimetric assays described above, biosensing based on the optical scattering properties of plasmonic nanoparticles is regarded as a potentially more powerful method. One technique that exploits the scattering optical properties of noble metal nanoparticles is dark-field optical microscopy. Allowing the visualization of individual particles [12], dark field microscopy has been widely used to image nanoparticles uptake by cells, while others combined it with the LSPR shifts associated with local dielectric constant changes to produce *light scattering biochips* for analyte detection.

Chapter 2

2.1 Gold nanospheres synthesis and conjugation with chitosan biopolymer

2.1.1 Nanoparticles synthesis and biofunctionalization with chitosan

Gold nanoparticles were synthesized by an environmentally benign approach that uses L-ascorbic acid as gold salt reducer at room temperature. To increase AuNPs stability, we used chitosan biolopolimer, already proved for its capabilities as gold nanoparticle stabilizer by involving steric hindrance instead of conventional electrostatic stabilization [13].

2.1.2 Characterization of chitosan-capped gold nanoparticles

2.1.2.1 Morphological and Spectroscopic characterization

A first indication on the chitosan-capped gold nanoparticles formation was the colloidal solution pinkish-red color, known to be related to the excitation of gold nanoparticles SPR and was verified by UV-Vis extinction (absorbance plus scattering) spectroscopy measurements. The extinction spectrum of chitosan-capped AuNPs is illustrated in figure 2-1A (full line) and presents a maximum at 530 nm. Typically, standard citrate-capped gold nanospheres of 18 nm diameter display a single extinction band in the visible spectral region at 520 nm when measured in aqueous solution [14] (figure 2-1A dotted line).

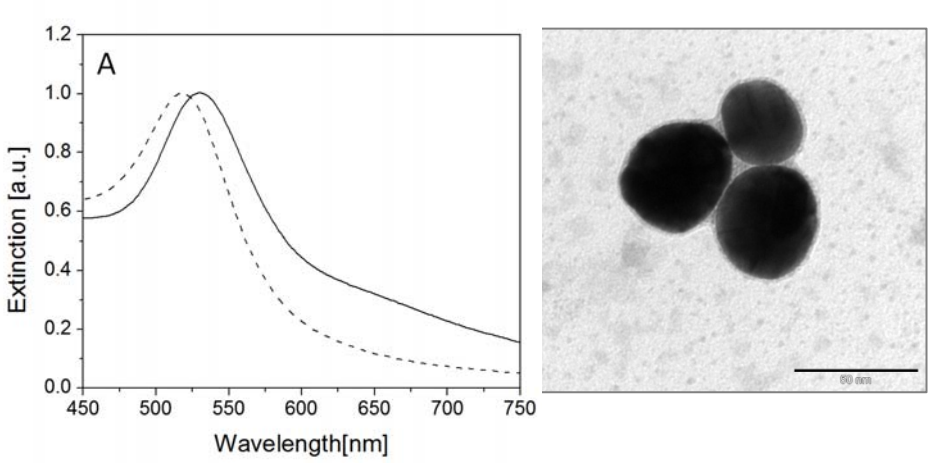

Fig. 2-1 A) Vis extinction spectrum of 50 nm chitosan-capped gold nanoparticles (full line) compared with 20 nm citrate gold nanospheres. TEM image of several gold nanoparticles of about 50 nm diameter, embedded in a 3 nm chitosan polymeric layer. Scale bar 50 nm.

2.2 Gold nanoflowers synthesis and biofunctionalization with mPEG-SH

2.2.1 Synthesis of gold nanoflowers

By adjusting the synthesis parameters, while keeping the same reactants as the ones used in the synthesis of nanospheres (L-ascorbic acid, having the role of gold salt reducer and tetrachloroauric acid ($HAuCl_4$) used as nanoparticle initiator), we fabricated gold nanoparticles of anisotropic, flower-like shape.

2.2.2 Morphological characterization of gold nanoflowers

The structure and size distribution of as prepared nanoparticles were determined by transmission electron microscopy (TEM) and scanning electron microscopy (SEM) measurements. Figure 2-2A shows TEM images of nanoparticles which resemble flowers. SEM image in figure 2-2B reveals more clearly the morphological structure of nanoparticles. We observe that they consist of a solid gold core of about 40 nm with many short, irregular petals (protrusions) of 10 nm average size.

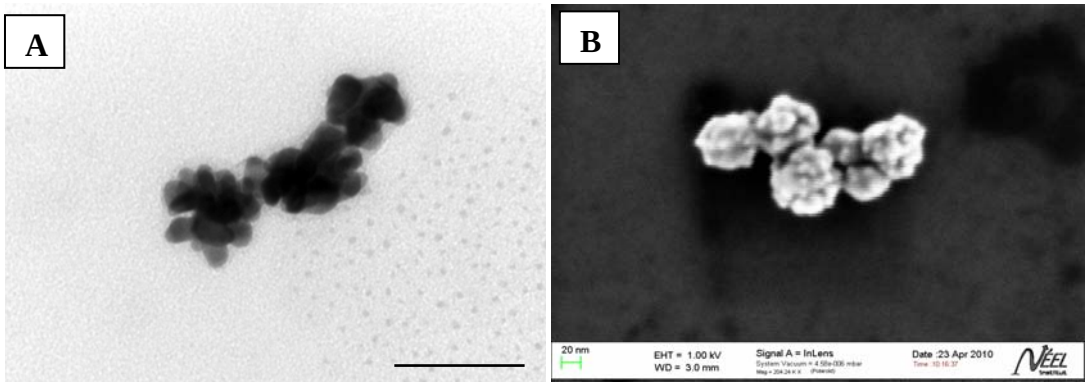

Fig.2-2 TEM (A) and SEM (B) mages of flower-shaped gold nanoparticles. Scale bars 50 nm and 20 nm respectively.

2.2.3 Spectroscopic characterization of gold nanoflowers

The optical properties of flower-shaped nanoparticles were investigated by Vis-NIR extinction spectroscopy measurements at the end of synthesis process. The extinction spectrum of dim blue colloidal solution is illustrated in figure 2-3. The plasmon band situated at 605 nm is visibly enlarged and asymmetric towards the NIR region of the spectrum, being consistent with previous examples from literature [15]. The spherical nanoparticles of 50 nm diameters present their LSPR band at 530 nm while star shaped

or branched nanoparticles with tips of 30 nm usually present two bands, one around 500 nm and another band at about 700 nm. As the LSPR band measured in this study extends between that of spherical and star shaped particles, the gold nanoflowers reported here can be fairly regarded as hybrids of stars and spheres.

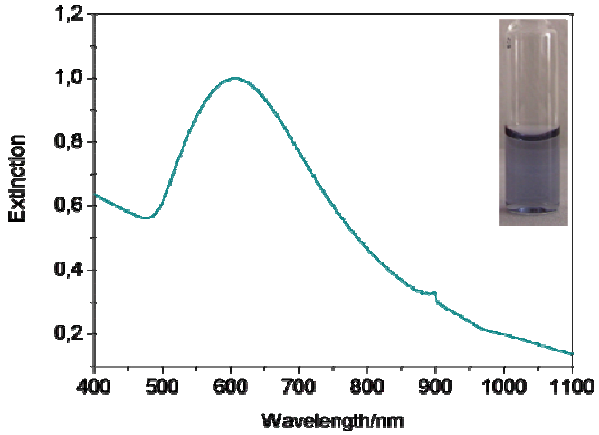

Fig.2-3 Normalized extinction spectrum of gold nanoflowers (GNFs) in aqueous solution.

2.2.4 Conjugation of gold nanoflowers with Poly(ethylene) glycol

Most of the colloids prepared by one-pot aqueous reduction of tetrachloroauric acid are stably dispersed in aqueous solution through ionic repulsive forces. However, such electrostatic stabilization is not always fully satisfied, therefore supplementary protective species are added to the colloidal solution. In our design, we have chosen thiolated Poly(ethylene) glycol (mPEG-SH) polymer to improve the non-fouling character of as prepared GNFs and the colloidal stability.

Comparative extinction spectra of the colloids were subsequentely measured to characterize the nanoparticles. The extinction spectra of uncoated (dashed line) and PEGylated (full line) gold nanoflowers are illustrated in figure 2-4A. A red shift of 11 nm together with a slight band enlargement was observed for PEGylated nanoparticles. This redshift can be explained by the increase of the refractive index surrounding the nanoparticles when PEG tethered chains were constructed onto the gold nanoparticles surface. The effective nanoparticles capping by PEG was further confirmed by TEM images (figure 2-4B), which reaveal the polymeric layer of about 5 nm thickness surrounding the nanoparticles as a corona.

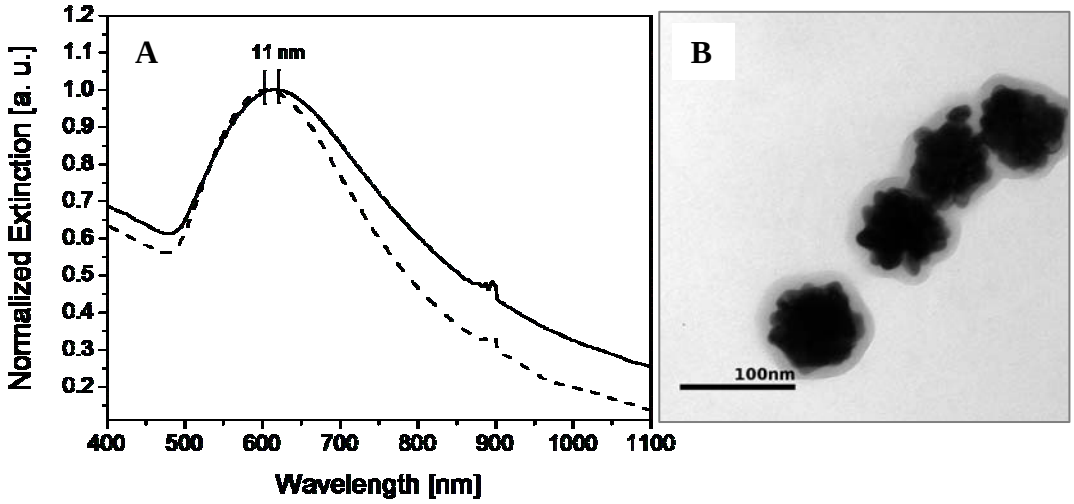

Fig.2-4 A) Normalized extinction spectrum of uncoated (dashed line) and PEG-coated (full line) gold nanoflowers (GNFs) in aqueous solution. **B)** TEM images of several gold nanoflowers capped with a 5 nm layer of PEG polymer

2.3 Gold nanorods synthesis, detoxification and biocompatibilization with mPEG-SH

2.3.1 Gold nanorods synthesis and PEGylation

Several synthesis methods exist to prepare metallic nanorods such as electrochemical, pohotchemical, microwave heating or seed-mediated growth [16]. Herein, we employed the seed-mediated growth approach at room temperature developed by Jana *et al* to synthesize gold nanorods with aspect ratios (length/width) up to 3.7. For gold nanorods PEGylation, a solution of mPEG-SH in ddH_2O was first prepared. Several μL of the polymeric solution were added to an appropriate volume of colloidal gold nanorods. The sample was kept overnight at room temperature to allow the polymer to bind onto nanorods surface, then was submitted to another centrifugation step which removed the supernatant containing unbounded polymer and other reactants. The nanorods pellet was resuspended in ddH_2O and remained stable for several months at room temperature.

2.3.2 Characterization of mPEG-SH capped gold nanorods

Gold nanorods detoxification and functionalization was monitored by employing three different techniques: optical extinction, TEM imaging and SERS. For nanorods functionalization we selected the shorter ones, having an aspect ratio of 2.5 (80 nm/32 nm), due to the fact that this size (<100 nm) approaches the size of biomolecules and

therefore the particles can have a higher uptake by the cells. The spectrum presents two extinction bands, situated at 519 nm and at 632 nm for the transversal and longitudinal modes respectively. Adding mPEG-SH into gold nanorod solution did not greatly affect their optical properties. However a 3 nm red shift of the longitudinal band was observed for PEGylated particles, and a slight decrease of the extinction intensity (figure 2-5 A).

The presence of the polymer around the particles was also confirmed by TEM imaging. Figure 2-5B presents a selected nanorod from the initial solution and a PEGylated particle for comparison. For the coated particle, the polymer clearly appears as a faint uniform layer of approximately 4 nm around the darker nanorod [17].

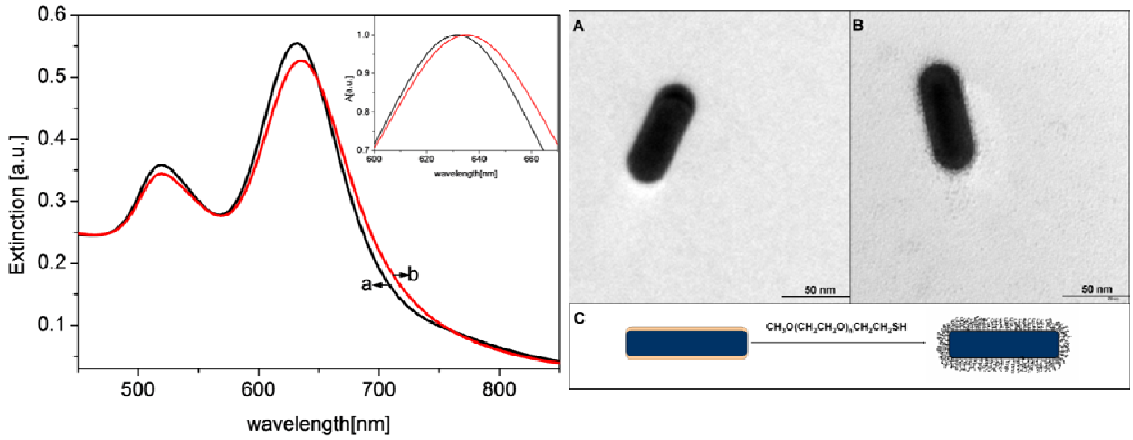

Fig.2-5 UV-Vis-NIR extinction spectra of gold nanorods of 2.5 aspect ratio: **(a)** raw GNRs; **(b)** mPEG-SH-conjugated GNRs. Inset: magnification of the normalized longitudinal extinction bands.

Chapter 3

3.1 Probing DNA-gold nanoparticles interaction by colorimetric spectroscopic detection

3.1.1 DNA-gold nanoparticles conjugates preparation

Spherical gold (Au) nanopaticles of approximately 20 nm were synthesized by Turkevich method described in the following lines. The stabilization of Au nanoparticles was made by adding ssDNA with the following sequence: 5'-GGA CTC GAG TTA CTC TTT TAT GTT CCA CTTC-3' solution to gold colloid. The samples were aged for 10 minutes and in a second exeperiment, for three days. For aggregation tests, a solution of NaCl was introduced in the cuvettes containing the mixtures of gold colloids and the oligomers.

The prepared solutions were kept at room temperature for three days and after this period, optical absorbance measurements were employed.

3.1.2 Spectroscopic detection of DNA-gold nanoparticles interaction by colorimetric tests

In the first experiment we mixed the colloidal nanoparticle solution with single and double stranded DNA and aged the samples for 10 minutes. After this period we added salted solution to test nanoparticles stability. A first ochimetric observation was that all the samples changed color from red to blue immediately after the NaCl solution was introduced, indicating the aggregation of the particles. This was confirmed by UV-vis extinction measurements.

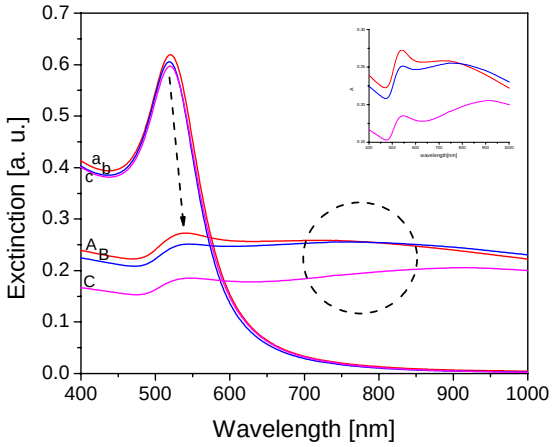

Fig.3-1 Extinction spectra of gold colloids mixed with: a- ssDNA; A-ssDNA with NaCl solution; b-ssDNAc; B- ssDNAc with NaCl; c- dsDNA; C- dsDNA with NaCl; the solutions were aged for 10 minutes.

Based on the results obtained in the previous exeperimet, in the second attempt we modified time parameter from ten minutes to three days while keeping the rest of the eperimental conditions identical. Different results were obtained for the samples incubated with ssDNA [18].

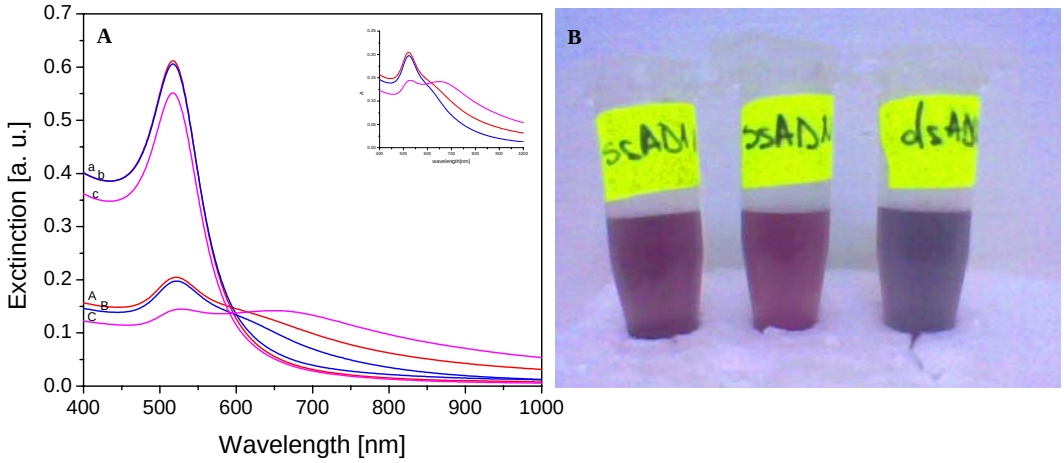

Fig.3-2 A) Absorbance spectra of gold colloids mixed with: a ssDNA; A-ssDNA with NaCl solution; b-ssDNAc; B- ssDNAc with NaCl; c- dsDNA; C- dsDNA with NaCl; the solutions were aged for 3 days. **B)** Photographic image of gold colloid mixtures with (from left to right): ssDNA, ssDNAc and dsDNA after being incubated with NaCl solution.

In this case, the colloidal solution maintained its specific red color after the addtion of salt. This demonstrated an efficient stabilization of the samples through binding between the single stranded DNA sequances onto gold nanoparticles surface. Sample incubated with dsDNA changed color from red to blue after the adding of NaCl, denoting unsufficient stabilization of the particles.

3.2 Gold nanospheres for Surface Enhanced Raman Spectroscopy detection

3.2.1. Samples preparation

Colloidal gold NPs of 18 nm were synthesized by the aqueous reduction of $HAuCl_4$ with trisodium citrate according to the Turkevich method described previously. Further, nanoparticles were immobilized on silanized glass slides to fabricate SERS-active substrates.

3.2.2 Optical and morphological characterization

Gold (Au) particles and the clusters they formed are adsorbed on glass slides due to electrostatic interactions between the positively charged amino terminated groups of APS that are on the functionalized glass surfaces and the citrate anions presented on the nanoparticle surface. Figure 3-3A shows the optical absorbance spectra of the self-assembled gold SERS substrates. While in the case of fresh colloidal solutions there is

only one surface plasmon band which was attributed to isolated particles, the prepared nanostructured substrates present also a longer wavelength broad band corresponding to collective surface plasmon modes excited on the aggregates. The clusterization of gold colloids into aggregated structures which are then adsorbed on glass substrates was also verified by AFM investigations. As can be seen in Figure 3-3B Au nanoparticles of 18 nm are assembled into an almost uniform monolayer while in the rest of the images one can observe an insular topography.

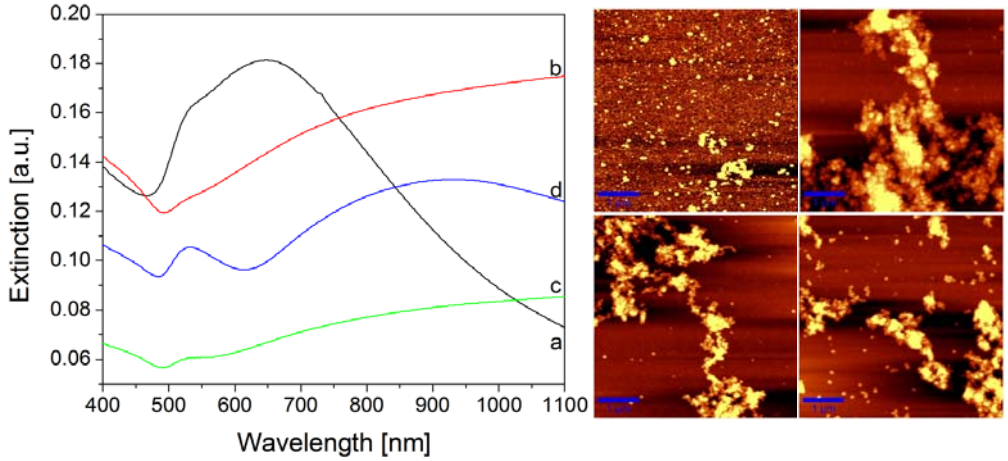

Fig.3-3 UV-Vis absorption spectra of self-assembled Au NPs on glass slides: (a) 18 nm, (b) 30 nm, (c) 40 nm and (d) 75 nm gold nanoparticles on silanized glass substrates. AFM images of self-assembled Au NPs on glass sildes: (A) 18 nm, (B) 30 nm, (C) 40 nm, and (D) 75 nm.

3.2.3 Colloidal self-assembled probes as SERS substrates using p-ATP molecule

We recorded optical spectra of the samples after p-ATP incubation and we concluded that adsorbtion of p-ATP molecules on the aggregated NPs films caused negligible spectral changes. Figure 3-4 presents a representative set of SERS spectra of p-aminothiophenol molecules adsorbed on different topography gold nanoparticle films. The intensity of the two dominating a_1 vibrational modes of p-ATP molecules at 1078 and 1588 cm^{-1} is indeed increasing with the size of NPs forming the aggregates. We have to mention that we collected series of SERS spectra from different points on each sample and bands positions and intensities are highly reproducible.

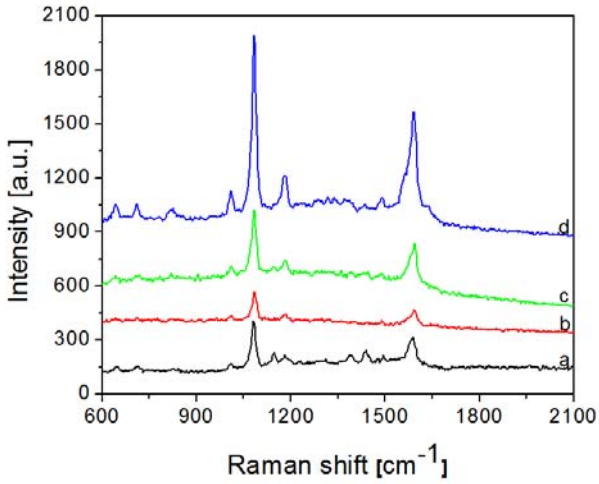

Fig.3-4 Surface enhanced Raman spectra of p-aminothiphenol adsorbed on different sized Au NPs samples: (a) 18 nm, (b) 30 nm, (c) 40 nm, and (d) 75 nm.

It should also be noted that the morphologies of the aggregates, as probed by AFM, are similar in the clustered samples. All the aggregates have a self-affine cluster-like structure, and the numbers of nanoparticles per aggregate are similar in the different samples. This actually implies that the particle density on the substrates decreases by a factor approximately $(D_1/D_2)^2$ between two samples made of NPs with diameter D_1 and D_2 respectively (if $D_1 < D_2$). The number of molecules per nanoparticle is proportional to the particle surface area and increases by a factor $(D_2/D_1)^2$ from the D_1 to the D_2 sample. Therefore both samples have approximately the same number of molecules per unit substrate area. It was very recently demonstrated that measured SERS signals are dominated by the signal of a small percentage (<1%) of all the probed molecules. It is conceivable that these molecules are located at hot-spots formed in junctions between NPs. In our samples the hot-spots are randomly distributed within the colloidal aggregates. Due to the similar morphology of the aggregates we expect that the hot-spots bring a similar contribution to the overall measured SERS spectra. Therefore the different enhancements exhibited by the different studied samples can be attributed only to intrinsic size effects, related to different EM field enhancement factors on NPs of different sizes [19].

Chapter 4

4.1 Dye-encoded gold nanoflowers as SERS tags

4.1.1 SERS-tags preparation

For nanoparticles conjugation, malachite green oxalate (MG) and basic fuchsin (BF) solutions were added dropwise to a few mL of nanoparticle solutions and shacked for several minutes as schematically illustrated in figure 4-1. The Raman reporter molecules concentration and nanoparticle binding time was carefully established to achieve enough reporter molecules/particle without causing a severe nanoparticle aggregation.

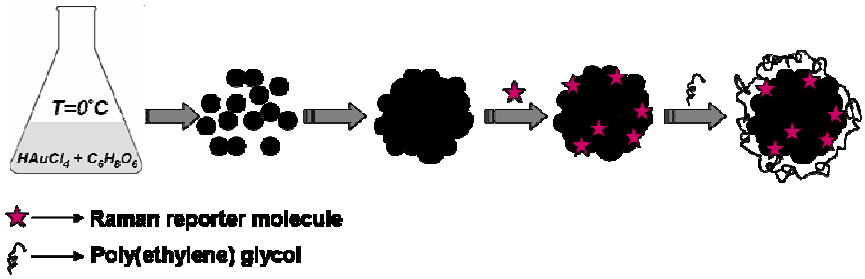

Fig.4-1 Representation of Raman tags preparation process

4.1.2 Particle stability measurements

We first compared the optical extinction spectra recorded before and after nanoparticle tagging (colored thick curves) and untagged (black curves). In figure 4-2A the two spectra look almost identical. Few nm red-shift of plasmonic resonance is observed for MG-tagged nanoparticles which is consistent with a local change in the optical refractive index due to electrostatic interaction between the cationic reporters and the negatively charged nanoparticles. A more pronounced effect can be observed for BF-tagged gold nanoflowers whose plasmon band is visibly enlarged and 15 nm red-shifted after adding the reporter molecules. Although both MG and BF possess the electronic transition in this spectral region, their molecular absorption bands are not detectable at this low concentration (less than 10^{-7} M), being practically masked by the Au plasmon extinction band.

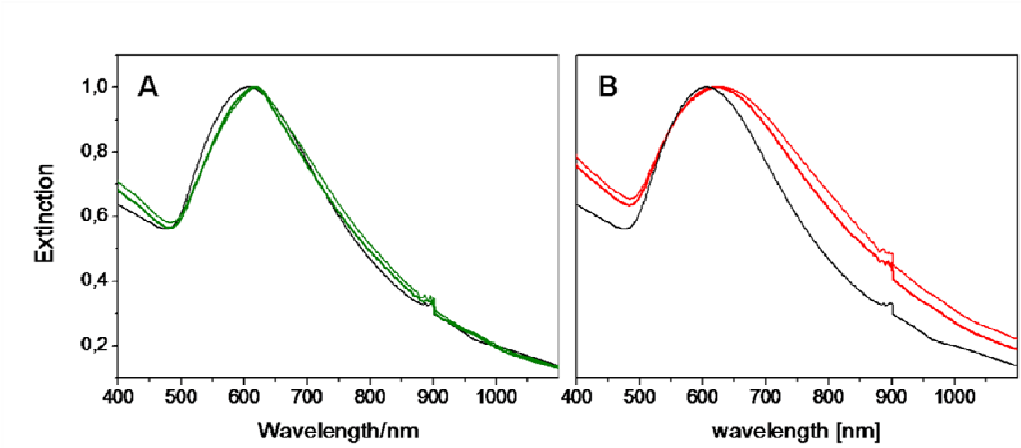

Fig.4-2 Extinction spectra of gold nanoflowers recorded in the absence (thick lines) and in the presence (thin lines) of 1 M salted solution. Black lines represent uncoated particles while colored (green for MG-GNFs and red for BF-GNFs) represent tagged particles.

4.1.3 Dye- encoded gold nanoflowers as SERS-tags

The SERS applicability of flower-shaped nanoparticles was investigated for two molecules with affinities for the negative charged nanoparticle gold surface, malachite green oxalate and basic fuchsin. Figures 4-3A and 4-3B show the SERS spectra of PEGylated malachite green (MG-GNFs) and basic fuchsin (BF-GNFs) tagged nanoflowers respectively, recorded in solution using 785 nm NIR excitation. The SERS spectra exhibit characteristic vibrational bands of the two molecules, which are clearly distinguishable, irrespective of the closely similar molecular structure of the two triarylmethane chromophores.

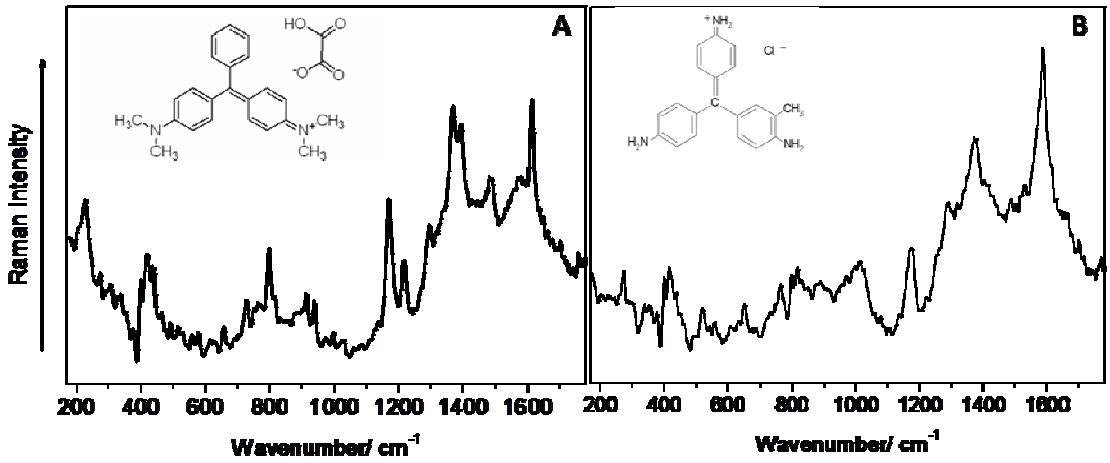

Fig.4-3 SERS spectra of malachite green (A) and basic fuchsin gold nanoflowers (B) in solution recorded under 785 excitation.

4.1.4 Intracellular SERS detection using gold nanoparticles

To demonstrate the reliability of our SERS tags, we incubated D407 cells in the presence of PEGylated BF-encoded gold nanoparticles for 24 h. Figure 4-4A shows two SERS spectra which highly resemble: the Raman-encoded particles signature collected as reference from a colloidal solution (spectrum ii) and the spectrum collected from inside the cells from where the nanoparticles were internalized (spectrum iii), as can be seen in the optical image in figure 4-4B. No Raman signal could be obtained from nonloaded cells or from nuclear free of particles region for loaded cells (spectrum i). These results, supplementary prove that our encoded nanoparticles are highly stable and protected from protein adsorption, being able to conserve their Raman identity in vitro, and therefore amenable to future spectral imaging applications inside living organisms [20].

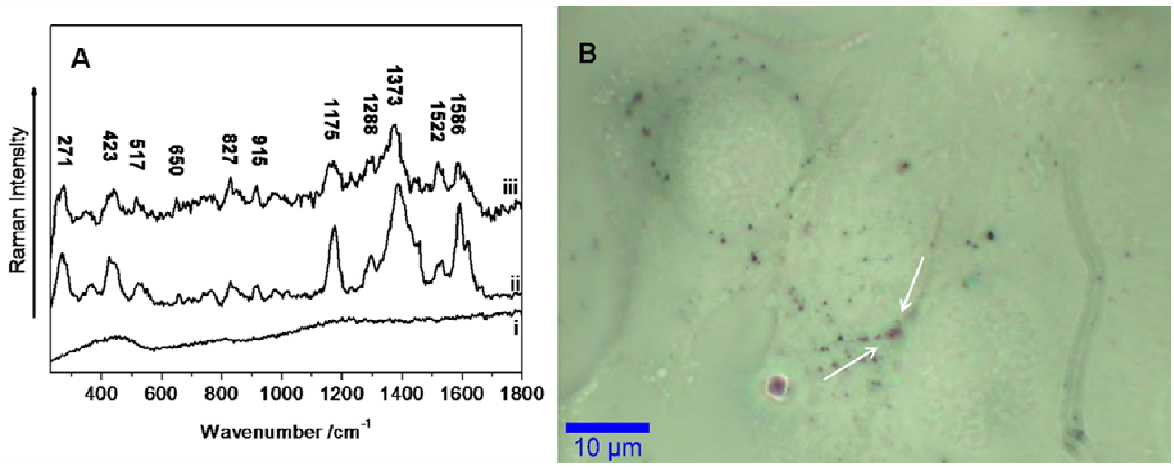

Fig.4-4 (A) SERS spectra of as prepared BF-GNFs in aqueous solution (ii), inside one selected region (marked by arrows) of a cell (iii) and from cells free of particles (i) recorded under 633 nm exicitation. The spectra are baseline corrected for better visualisation. (B) Transmitted light optical image of three D407 cells loaded with Raman-encoded gold nanoflowers.

Chapter 5

5.1 Nanoparticles cellular uptake and release studies

5.1.1 Bright and darkfield microscopy imaging

In our study the nanoparticles uptake by the cells was determined using dark field and phase contrast microscopy. Figure 5-1 presents the light scattering images of chitosan-silver nanotriangles (A) and PEG- gold nanorods (B) after binding to malignant HTB177 cells. Both types of nanoparticles appear to be reddish, due to resonantly scattered light around the surface plasmon wavelength at 750 nm. We also noticed that the noble metal nanoparticles did not photobleach or blink over time, as it happens often with other imaging agents such as fluorescent molecules or quantum dots [21].

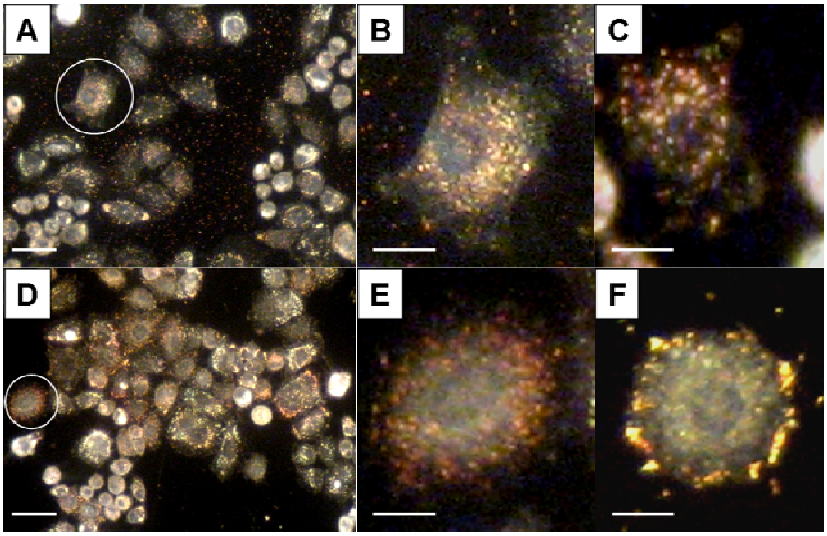

Fig.5-1 Dark field microscopy images of HTB177 cancer cells incubated with Chit-AgNTs (A, B, C) and PEG-AuNRs (D, E, F). The corresponding images of a magnified cell in each sample visualised after 2 hours (B, E) and after 24 hours (C), (F) incubation in the presence of the particles. Both types of nanoparticles scatter red light due to the plasmonic resonance at about 750 nm. Scale bars 20 nm (A, D) and 10 nm (B, C, E, and F).

5.2 Cellular viability studies in the presence of nanoparticles

5.2.1. Cell viability assessment in the presence of PEG-capped gold nanorods and Chit-AgNTs

Comparative studies were also conducted to test the impact of PEGylated annorods and ChitAgNTs onto cells. In this regard two different lines of cells: Human Embryonic

Kindney (HEK) nontumoral and Human Lung Carcinoma (HTB177) tumoral cells were used. Preliminary tests were made by incubating the cells in the presence of similar concentration of nanoparticles and then observing any morphological changes based on our recently reported viability studies [22]. Two supplementary cell samples were used as positive (cells without nanoparticles) and negative (CTAB-AuNRs) control.

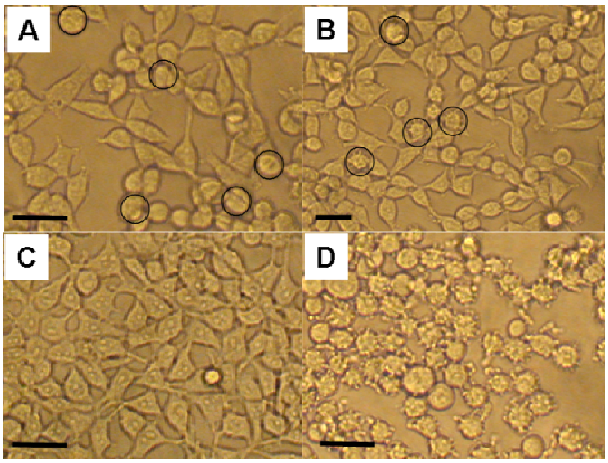

Fig.5-2 Phase contrast images of HEK cells after 24 h incubation with Chit-AgNTs (A) and PEG-AuNRs (B). Images (C) and (D) represent positive (cells with no particles) and negative (cells with CTAB toxic AuNRs) control samples. Scale bars 20 μm.

5.2.2 Colorimetric exclusion by fluorescence microscopy

More accurate viability studies were made using the double Hoechst-PI dye staining technique. By this, we wanted to determine the toxicity threshold value for each type of nanoparticles. Nuclear staining revealed that, at the used concentrations, chitosan-coated silver nanotriangles present higher biocompatibility for HEK healthy cells than PEG-AuNRs, since more than 95% of the total cells remained viable after 24 h incubation in the presence of highest nanoparticle concentration (figure 5-3A). On the contrary, different effect was observed when testing the particles biocompatibility on cancer cells, for which Chit-AgNTs showed an interesing slight toxicity (figure 5-3B). In this case, the cell viability plots had similar features for the two types of nanoparticles, until a 1 μg/mL critical nanoparticles concentration in the case of Chit-AgNTs, starting from which, the percent of viable cells demonstrated an abrupt decrease until 75%. This intriguing result confirms other reported studies regarding the cytotoxic nature of silver nanoparticles towards cancer cells, even though herein the cytotoxic effect is visible from much lower

nanoparticles concentration, possibly due to a synergistic effect between silver and chitosan.

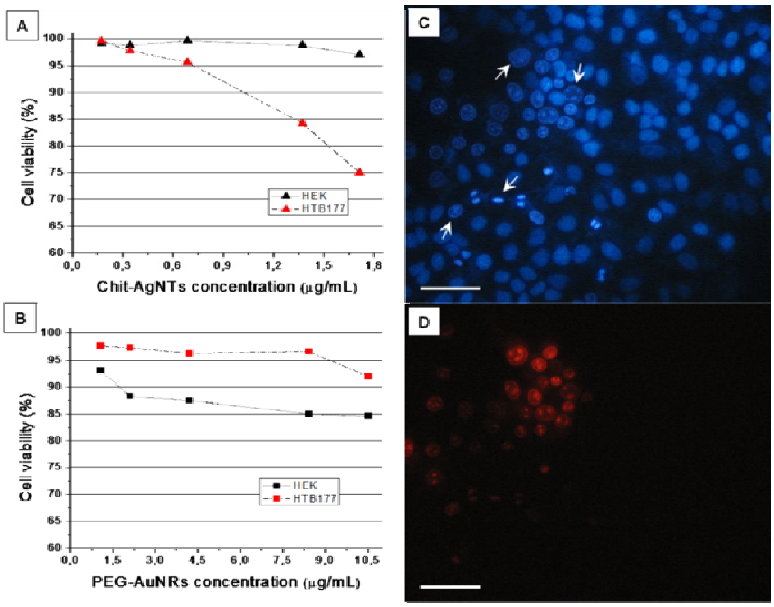

Fig.5-3 Cytotoxic profiles of Chit-AgNTs (A) and PEG-AuNRs (B) towards HEK (black symbols) and NCI-H460 (red symbols) cells. The cells viability is expressed as function of nanoparticles concentrations. Hoechst stained NCI-H460 viable cancer cells (C) and Propidium Iodide stained nonviable NCI-H460 cells (D) of the same cellular sample treated with Chit-AgNTs. The arrows indicate condensed and fragmented nuclei typical of apoptotic cells.

Chapter 6

6.1 Photothermal therapy of cancer cells using noble metal nanoparticles

6.1.1 Polymer-coated nanoparticles characterization

The normalized extinction spectrum of chitosan-silver nanoparticles in Figure 6-1, curve (a) exhibits four LSPR characteristic peaks corresponding to different modes of plasmon excitation on triangular silver nanoplates: two dipolar resonances at 724 nm (in-plane) and 449 nm (out-of-plane) and two quadrupolar resonances at 529 nm (in-plane) and 339 nm (out-of-plane), respectively. The reference sample exhibits (Figure 6-1, curve (b)) two LSPR characteristic peaks of gold nanorods, namely the transversal (at 519 nm) and longitudinal (at 758 nm) electron oscillation modes. It is relevant to point out that both nanoparticles are optically active in NIR by strong individual resonances located at 724 and 758 nm, respectively, and no induced aggregation would be required for excitation in NIR, as in the case of spherical nanoparticles.

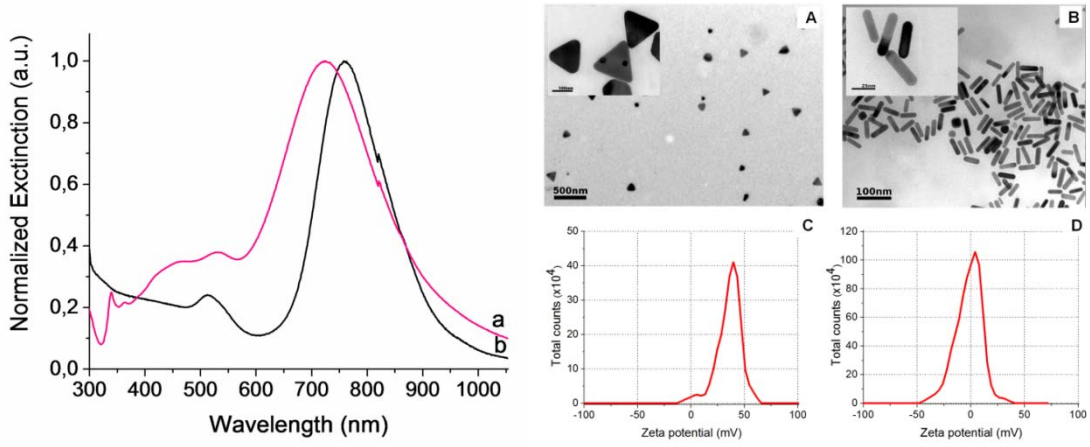

Fig.6-1 Normalized UV-Vis-NIR extinction spectra of Chit-AgNTs (spectrum a) and PEG-AuNRs (spectrum b) in aqueous solution. Transmission electron microscopy images of Chit-AgNTs (A) and PEG-AuNRs (B) and their corresponding surface charge distribution by ζ-potential measurements (images C and D). The insets of images A and B illustrate magnified TEM images of the same nanoparticles samples.

6.1.2 Plasmon assisted photothermal therapy

To determine whether as prepared nanoparticles can induce cellular death or not, we incubated the cancer cells in the presence of Chit-AgNTs and PEG-AuNRs and then irradiated the samples in resonance with the particles plasmon band. A control sample of cells without nanoparticles was irradiated under identical experimental conditions. Figure 6-2 shows the phase contrast images and the corresponding fluorescence images of HTB 177 cancer cells loaded with Chit-AgNTs (A) and PEG-AuNRs (B) and irradiated with 800 nm NIR CW laser at various laser intensities between 12 and 54 W/cm^2 for a fixed period of 10 minutes. A cellular death dependence on laser energy can be observed for both of the samples, the region of destroyed cells increasing with the laser intensity (see the marked regions in figure 6-2).

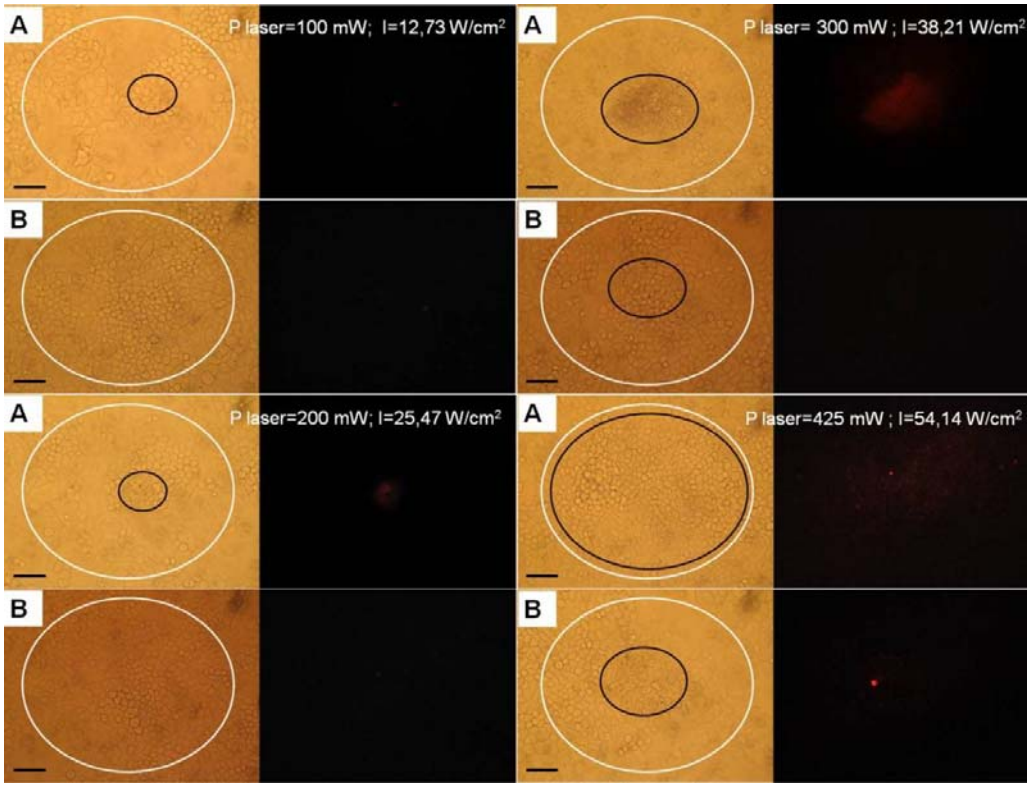

Fig.6-2 Phase contrast images and corresponding fluorescence images of NCI-H460 cancer cells loaded with Chit-AgNTs (A) and PEG-AuNRs (B) and irradiated with 800 nm NIR CW laser at various laser intensities. The white contour marks the irradiation spot while the black contour marks the destroyed cells zone. Scale bars 100 μm.

6.2 Photodynamic therapy of cancer cells using TEG decorated Ru(II) complexes

The UV-Vis absorption spectrum of RuPFPEG complex (Fig. 6-3) presents three bands, one between 250-300 nm ascribed mainly to the π-π* transitions of 1,10 phenanthroline ligand, another one between 330-350 nm which can be attributed to an absorption band centered on the oligofluorene and the band around 450 nm, corresponding to the long-lived metal-to-ligand charge-transfer (MLCT) excited states, important for the generation of singlet oxygen.

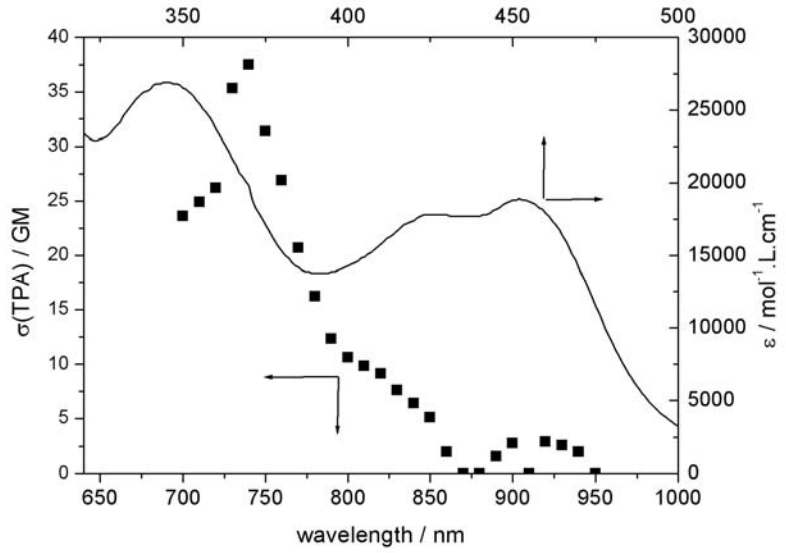

Fig.6-3 UV-Vis absorption and two-photon excitation spectra of the **RuL1TEG** complex, in $CHCl_3$ and CH_3Cl_3, respectively

6.2.1 In vitro fluorescence imaging

To achieve PDT, a first step was to demonstrate that the RuPFPEG complex can penetrate the cell membrane. In order to do that, we made several fluorescence imaging studies to noninvasively visualize the progression of the RuPFPEG complex into the regions of cytoplasmic vesicles. For fluorescence microscopy, F98 glioma cells were incubated for several minutes with the required molar concentration of RuPFPEG complex, and then the cellular medium was replaced with PBS solution. Fluorescence images were obtained both with 450 nm and 546 nm illumination. In the first case, the green fluorescence with an emission maximum around 550 nm, corresponds to the

protonated ligand, and in the second case, the red fluoresecence at 640 nm corresponds to the entire complex.

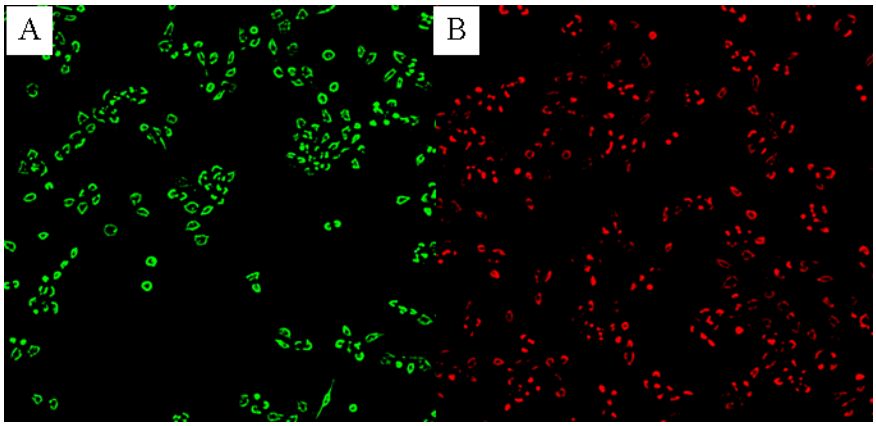

Fig.6-4 Fluorescence images of F98 cells loaded with the **RuL1TEG** complex. Excitation/emission wavelengths: (A) 450/490 nm and (B) 546/640 nm.

6.2.2 RuPFPEG complex used as phototoxic agent of living cancer cells, by two-photon absorption

RuPFPEG was specially designed to absorb two-photons, we selected it for two-photon photodynamic therapy of cancer cells. An image of a selected single cell, irradiated for five minutes with 300 mW output power of 740 nm pulsed laser line is presented in figure 6-5B in the circular region. We observe that the cell shape has a drastic modification from that before irradiation (figure 6-5A). This is a clear proof that the plasma membrane was harmed and that the targeted cell shrinked and died by means of $^1O_2$ toxicity [23].

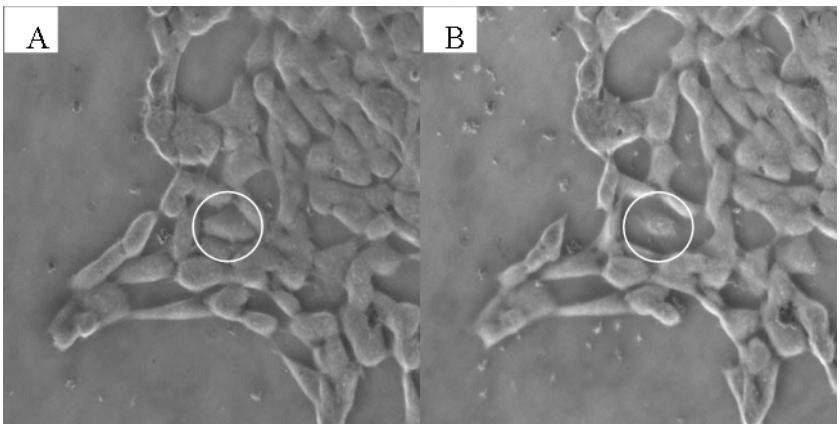

Fig.6-5 Phase contrast image of a single encircled F98 glioma cell before irradiation (A) and after 5 minutes of irradiation with 740 nm laser light (B).

Conclusions

In this thesis I prepared, characterized, studied the optical properties and demonstrated the aplicability of gold nanoparticles-polymeric conjugates in detection, intracellular imaging and cancer treatment by means of plasmonic assisted heating. Supplementary, I demonstrated the utility of newly synthesized photoactive molecules (herein Ru(II) complexes) in cancer imaging and photodynamic therapy.

1. **We fabricated gold nanoparticles of distinct and well-defined sizes (20-80 nm) and shapes (spheres, flowerlike, rods).**

2. **We succeeded to conjugate as prepared nanoparticles with (bio)polymers (Chitosan, Poly(ethylene) glycol-thiol) rendering them biocompatible.**

3. **We developed biosensing and spectroscopic detection (LSPR and SERS) application of gold nanoparticles.**

4. **We designed and characterized a class of spectroscopic encoded flower-shaped gold nanoparticles which can serve for intracellular SERS detection.**

5. **We studied nanoparticles uptake and toxicity onto various cell types, healthy and tumoral.**

6. **We demonstrated the efficiency of plasmonic nanoparticles in cellular cancer treatment by means of Plasmon Assisted Photothermal Therapy and ofphotoactive molecules in Photo Dynamic Therapy**

References

[1] Bair, F. E. Cancer Sourcebook: Basic Information on Cancer Types, Symptoms, Diagnostic Methods, and Treatments, Including Statistics on Cancer Occurrences World (Health Reference Series), Vol. 1, Omnigraphics, 1990.

[2] Miller, A. B.; Hoogstraten, B.; Staquet, M.; Winkler, A. Cancer 1981, 47(1), 207.

[3] T. J. Dougherty, C. J. Gomer, B. W. Henderson, G. Jori, D. Kessel, M. Korbelik, J. Moan, Q. Peng, Photodynamic Therapy, J. Natl. Cancer Inst., 90 (1998) 889-905.

[4] Chen, W. R.; Adamsc, R. L.; Carubellic, R.; Nordquist, R. E. Cancer Letters 1997, 115, 25.

[5] McBride, G. J. Nat. Cancer Inst. 2002, 94, 1740.

[6] G. Baronzio , G. Fiorentini, C. R. Cogle, Cancer Microenvironment and Therapeutic Implications, Springer Science+Business Media B.V. 2009

[7] http://encyclopedia.thefreedictionary.com/Colloidal+gold

[8] K. Lance Kelly, Eduardo Coronado, Lin Lin Zhao, and George C. Schatz, J. Phys. Chem. B 2003, 107, 668.

[9] J. Kimling, M. Maier, B. Okenve, V. Kotaidis, H. Ballot, A. Plech, J. Phys. Chem. B 110 (2006) 15700.

[10] Peter Johansson, Hongxing Xu, Mikael Kall, Phys. Rev. B 72, 035427 (2005).

[11] R.G. Rayavarapu, W. Petersen, C. Ungureanu, J. N. Post, T. G. van Leeuwen, S. Manohar, International Journal of Biomediacal imaging, 2007, Article ID 29817.

[12] Stefan A Maier, Plasmonics: Fundamentals and Applications, 2007 Springer Science+Business Media LLC

[13] Esumi K, Takei N and Yoshimura T, Colloids Surf. B 32 (2003) 117.

[14] P. K. Jain, K. S. Lee, I. H. El-Sayed, M. A. El-Sayed, J. Phys. Chem. B 110 (2006) 7238.

[15] K. Yu, K. L. Kelly, N. Sakai, T. Tatsuma, *Langmuir* **2008 ;** *24*, 5849.

[16] Jana N R, Gearheart L, Murphy C J 2001 *J. Phys. Chem. B* **105** 4065–4067

[17] Rui Hu, Ken-Tye Yong, Indrajit Roy, Hong Ding, Sailing He, and Paras N. Prasad, J. Phys. Chem. C, 2009, 113 (7), pp 2676–2684.

[17] Boca SC, Astilean S., Nanotechnology (2010) 21 Article number: 235601

[18] S. Boca, I. Lupan, O. Popescu, S. Astilean, Studia Universitatis Babes Bolyai, Physica, 1 (2008) 87.

[19] S. C. Boca, C. Farcau, S. Astilean, Nuclear Instruments and Methods in Physics Research: B , 267 (2009) 406

[20] Sanda Boca, Dumitrita Rugina, Adela Pintea, Lucian Barbu-Tudoran and Simion Astilean, Nanotechnology 22 (2011) Article number 055702

[21] Rui Hu, Ken-Tye Yong, Indrajit Roy, Hong Ding, Sailing He, and Paras N. Prasad, J. Phys. Chem. C, 2009, 113 (7), pp 2676–2684.

[22] Sanda C. Boca, Monica Potara, Felicia Toderas, Olivier Stephan, Patrice L. Baldeck, Simion Astilean, Mat. Sci. Eng. C., 31 (2011), 184.

[23] Sanda C. Boca, Mickael Four, Adeline Bonne, Boudewijn van der Sanden, Simion Astilean, Patrice L. Baldeck, Gilles Lemercier, Chemical Communication 30 (2009) 4590.